Doménfal elméleti vizsgálata egy kobalt pontkontaktuson keresztül

Balogh László, Palotás Krisztián, Lazarovits Bence,
Udvardi László, Szunyogh László

Budapest, 2011. október 28.

Tartalom

- Kísérleti előzmények
- Elméleti „modell”
- Számítások
  - Nemrelativisztikus leírás
  - Anizotrópia hatása
  - Módszer az alapállapot meghatározására
  - Az alapállapot energiaviszonyai

The Kondo effect in ferromagnetic atomic contacts I.

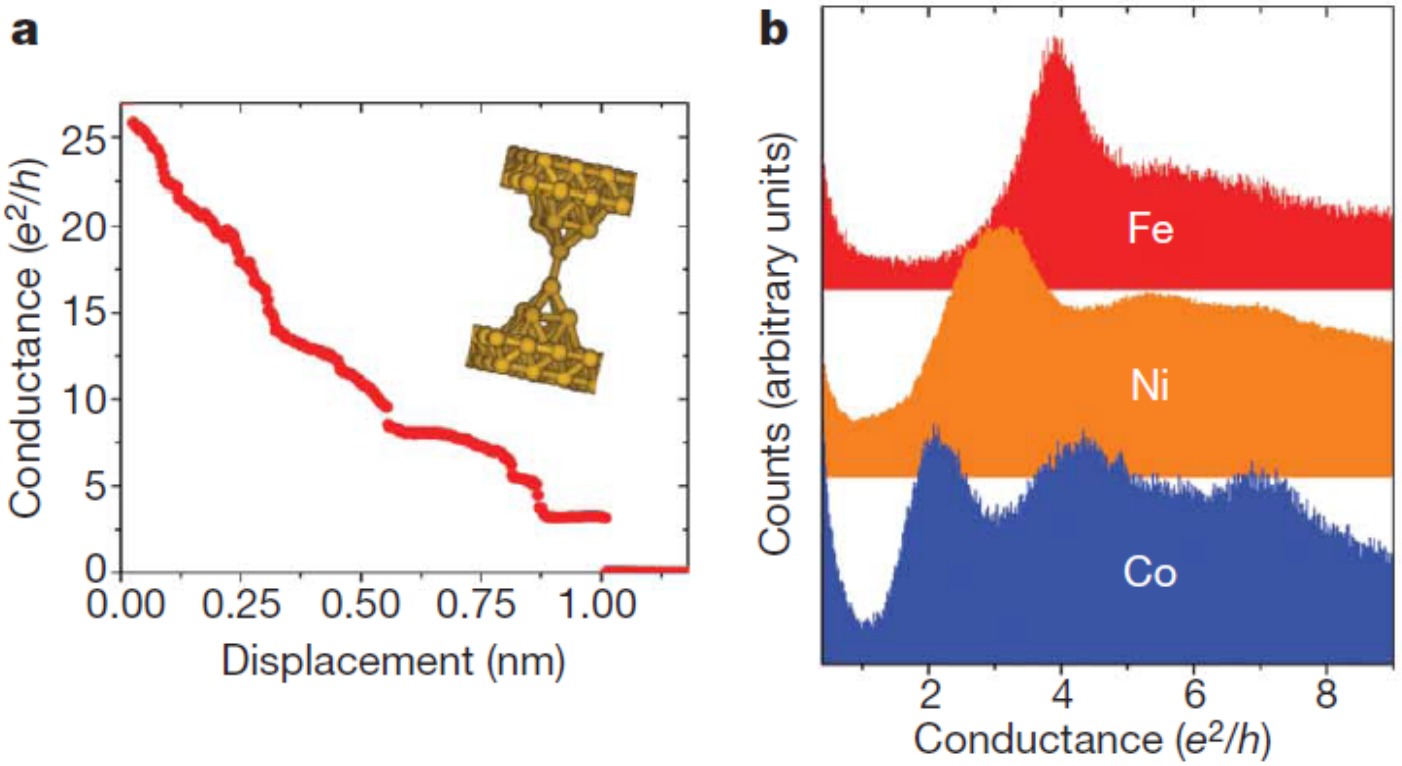

Figure 1 | Conductance of a monatomic contact. **a**, Example of a trace where we record the conductance while stretching a nickel wire using a scanning tunnelling microscope (STM) at 4.2 K. Inset, model of a monatomic contact. **b**, Conductance histograms constructed for iron, cobalt and nickel from thousands of such traces. The position of the first peak of in each histogram corresponds to the conductance of the monatomic contact. **c**, Differential

M. R. Calvo, *et al.,* Nature, **458,** 1150, (2009)

The Kondo effect in ferromagnetic atomic contacts II.

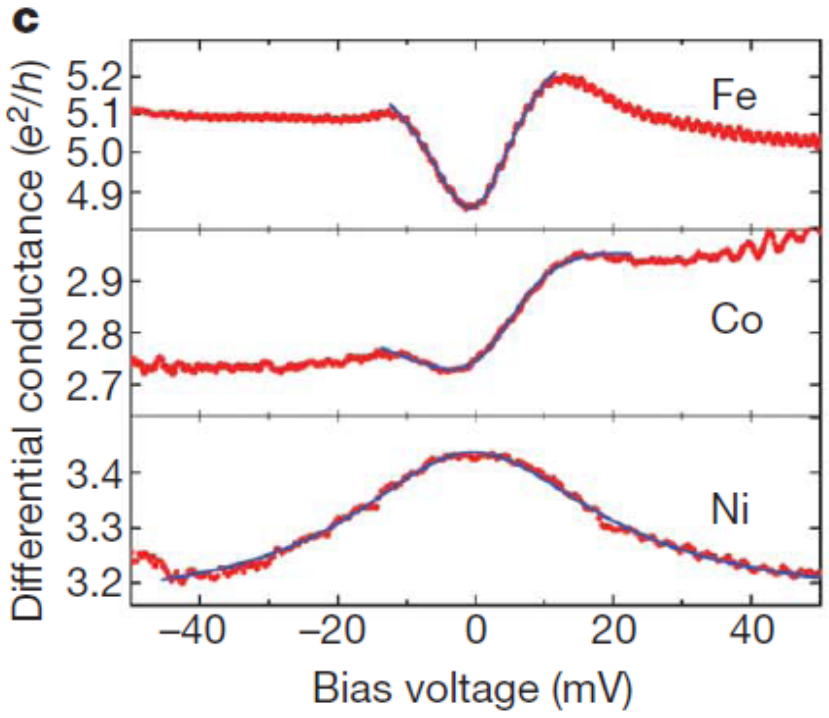

$$\frac{dI}{dV} = g_0 + \frac{A}{1+q^2}\frac{(q+\varepsilon)^2}{1+\varepsilon^2}$$

Here $\varepsilon = (eV - \varepsilon_s) / k_B T_K$ is the bias shifted with respect to the centre of the resonance, ε_s, and normalized by the natural width of the resonance, $k_B T_K$; T_K is the Kondo temperature; q is the dimensionless Fano parameter that determines the symmetry of the curve; A is the amplitude of the feature; and k_B is Boltzmann's constant.

c, Differential conductance curves recorded at the monatomic contact as a function of the applied voltage. A characteristic resonance appears at small bias that fits the Fano line shape. All possible symmetries are found in the spectroscopy of iron, cobalt and nickel contacts, and the width of the resonance is the main difference between the spectra of the three materials. This width is proportional to the Kondo temperature.

M. R. Calvo, *et al.,* Nature, **458,** 1150, (2009)

The Kondo effect in ferromagnetic atomic contacts II.

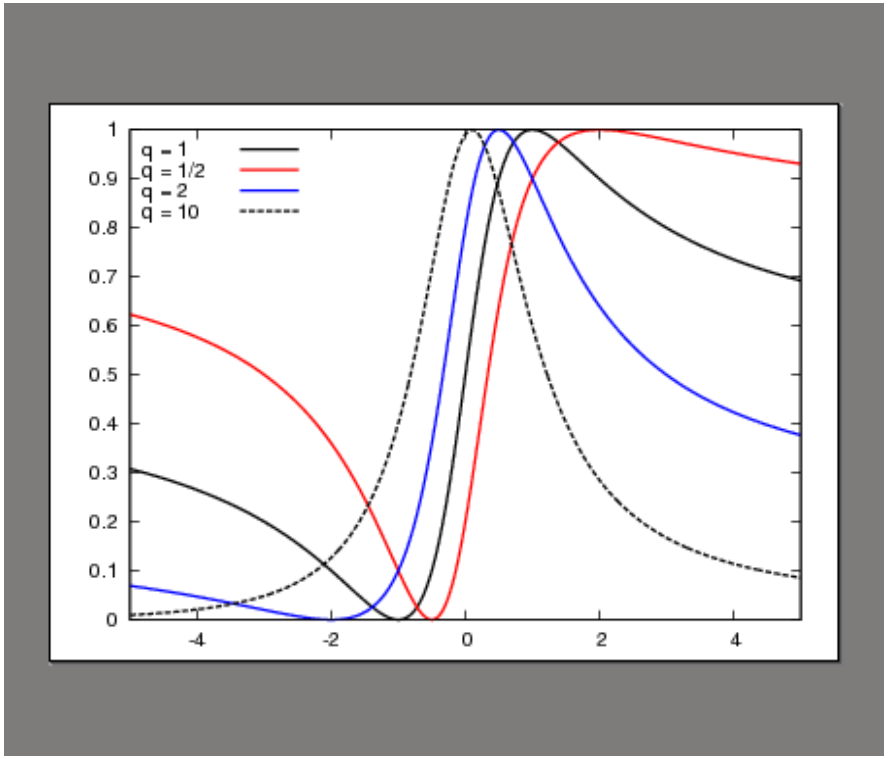

$$\frac{dI}{dV} = g_0 + \frac{A}{1+q^2}\frac{(q+\varepsilon)^2}{1+\varepsilon^2}$$

Here $\varepsilon = (eV - \varepsilon_s) / k_B T_K$ is the bias shifted with respect to the centre of the resonance, ε_s, and normalized by the natural width of the resonance, $k_B T_K$; T_K is the Kondo temperature; q is the dimensionless Fano parameter that determines the symmetry of the curve; A is the amplitude of the feature; and k_B is Boltzmann's constant.

c, Differential conductance curves recorded at the monatomic contact as a function of the applied voltage. A characteristic resonance appears at small bias that fits the Fano line shape. All possible symmetries are found in the spectroscopy of iron, cobalt and nickel contacts, and the width of the resonance is the main difference between the spectra of the three materials. This width is proportional to the Kondo temperature.

M. R. Calvo, *et al.,* Nature, **458,** 1150, (2009)

The Kondo effect in ferromagnetic atomic contacts III.

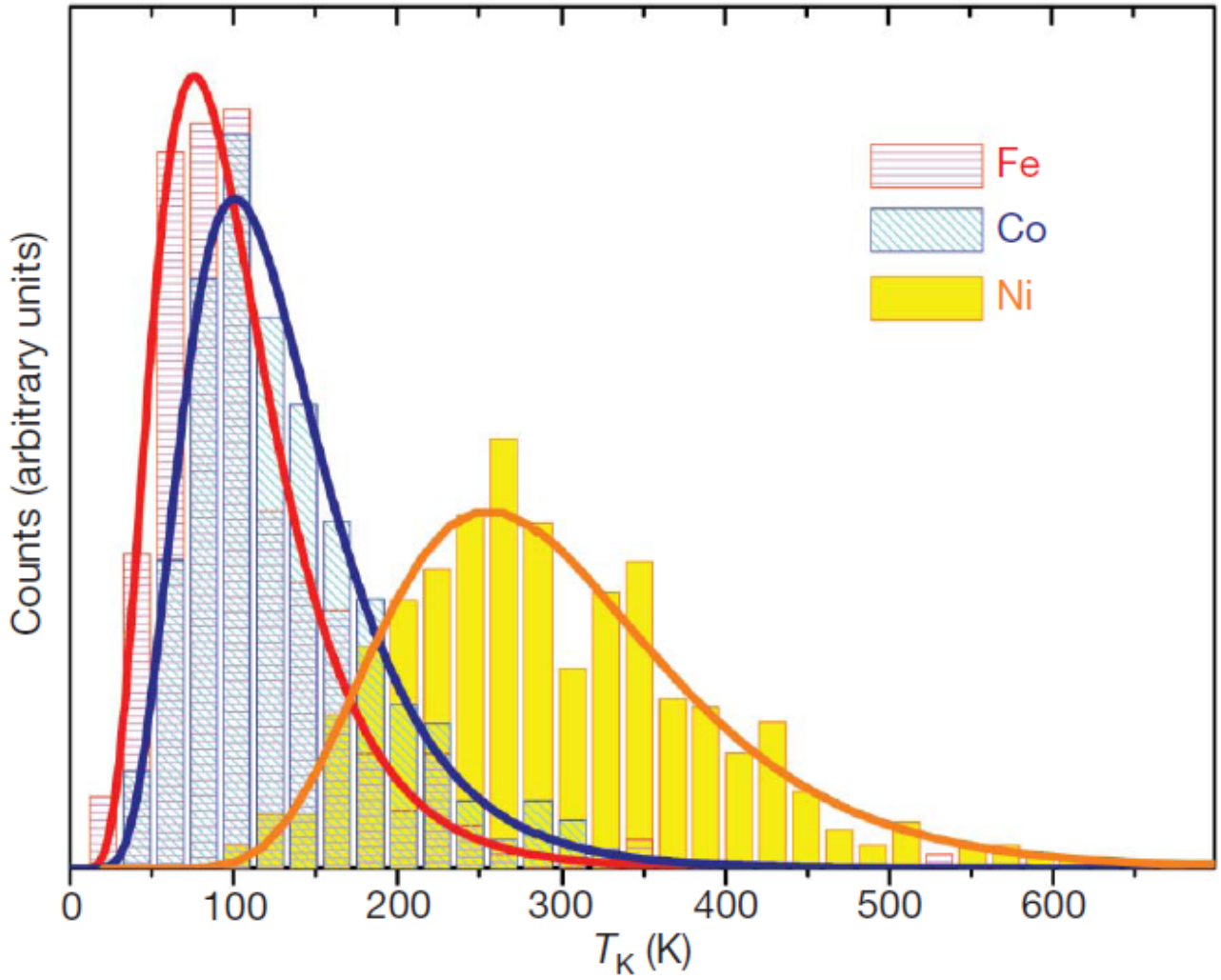

Figure 2 | Histograms of inferred Kondo temperatures for iron, cobalt and nickel. The histograms are constructed from more than 200 fittings and normalized to the total number of curves fitted. The continuous lines show the fits of the data to log-normal distributions of T_K with a different most probable value for each material.

M. R. Calvo, *et al.,* Nature, **458,** 1150, (2009)

Model system:

Co[001] + 3 x 3 + 2 x 2 + 1 + 1 + 1 + 2 x 2 + 3 x 3 + Co[001]

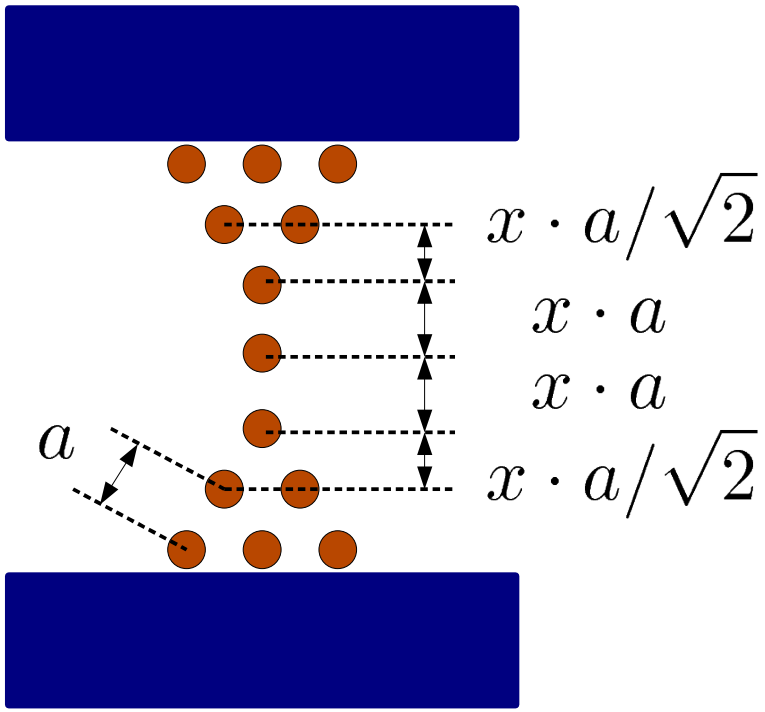

$x \in \{0.85, \ldots, 1.15\}$

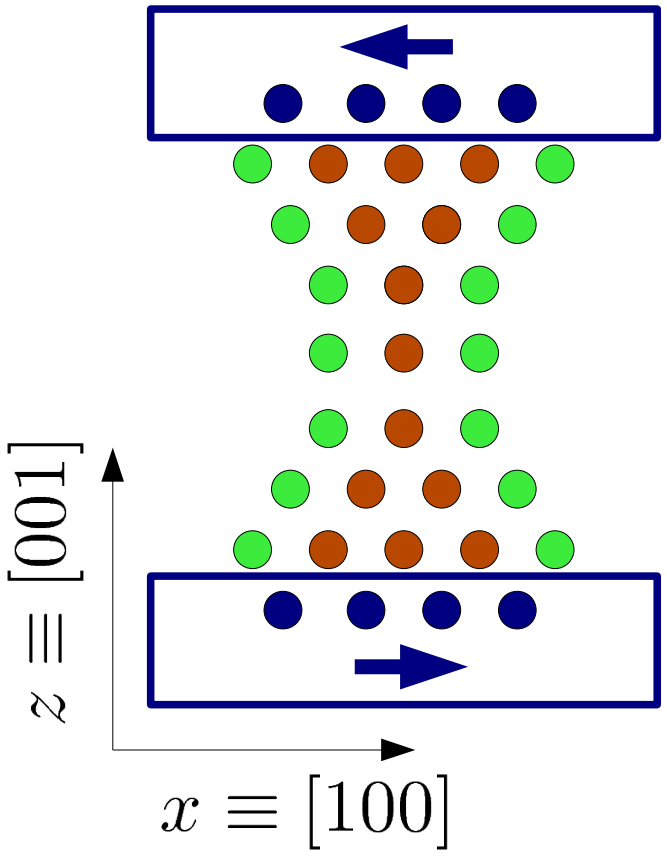

Atomic contact in antiferromagnetic environment in experiments

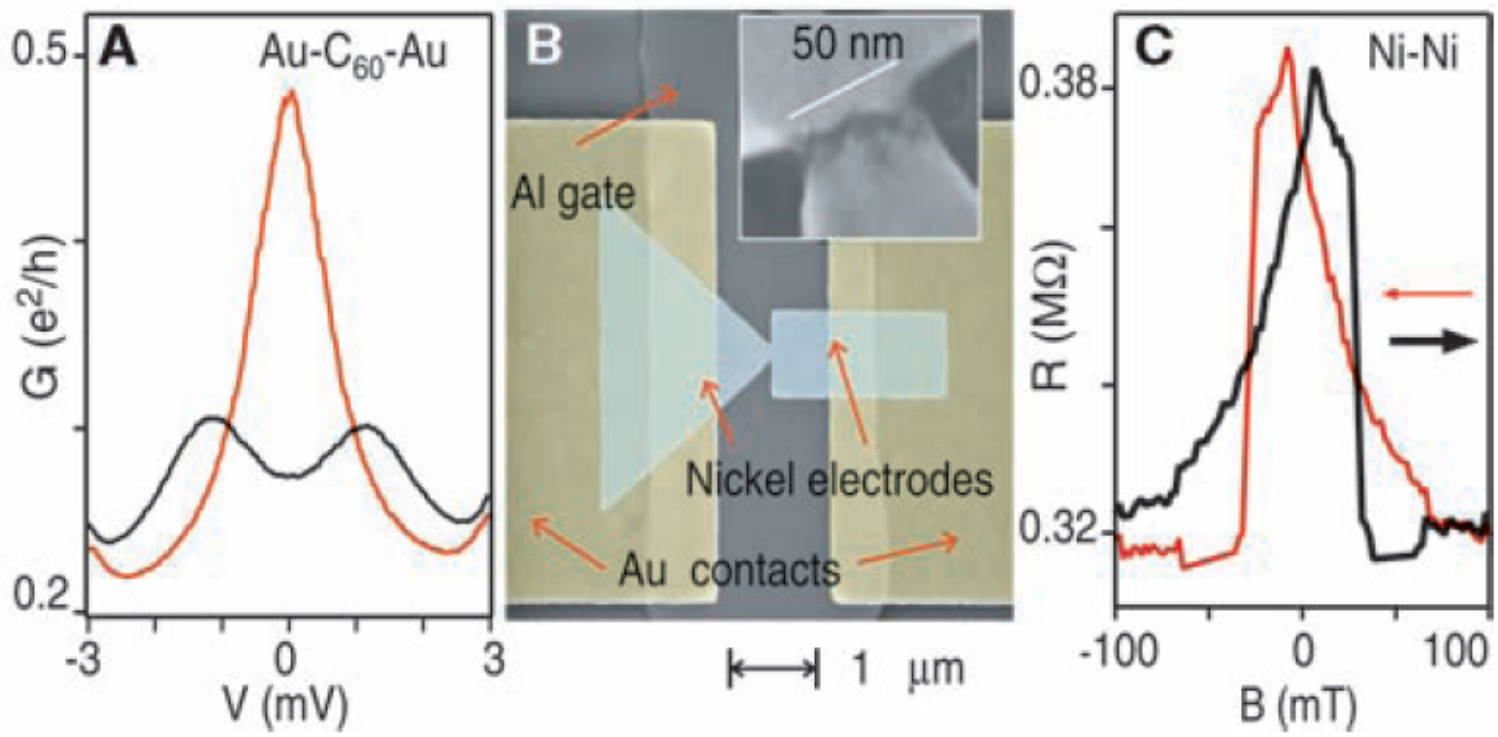

Fig. 1. (**A**) Kondo signal for C_{60} with Au electrodes at $T = 1.5$ K. At $B = 0$ (red line), there is a zero-bias peak in $G(V)$ that becomes split for $B = 10$ T (black line). (**B**) Scanning electron micrograph of a Ni break junction. The magnetic field is applied in the horizontal direction. (**Inset**) Close-up of the junction region after electromigration. (**C**) Tunneling magnetoresistance near $V = 0$ at $T = 4.2$ K of a Ni contact after electromigration, with no C_{60} molecule present.

A. N. Pasupathy, *et al.,* Science, **306,** 86, (2004)

Isotropic Heisenberg model

$$\mathcal{H} = \frac{1}{2} \sum_{i \neq j} J_{ij} \, \boldsymbol{\sigma}_i \cdot \boldsymbol{\sigma}_j$$

Invariant under global spin rotation.

Boundary condition: [100] and [$\bar{1}$00]

Invariant under global spin rotation around the [100] axis.

Configurations rotated around the [100] axis are equivalent.

Deficiensies of the isotropic Heisenberg model

Higher order terms, *e.g.,*

$$J_{\square}\left[\left(\boldsymbol{\sigma}_1\boldsymbol{\sigma}_2\right)\left(\boldsymbol{\sigma}_3\boldsymbol{\sigma}_4\right)+\left(\boldsymbol{\sigma}_2\boldsymbol{\sigma}_3\right)\left(\boldsymbol{\sigma}_4\boldsymbol{\sigma}_1\right)+\left(\boldsymbol{\sigma}_1\boldsymbol{\sigma}_3\right)\left(\boldsymbol{\sigma}_2\boldsymbol{\sigma}_4\right)\right]$$

(see: S. Lounis, P. H. Dederichs, Phys. Rev. B. **82**, 180404 (2010))

$$\mathbf{J}_{ij} \rightarrow \begin{cases} \mathbf{J}_{ij}^{\mathrm{I}} = \left(\frac{1}{3}\mathrm{Tr}\,\mathbf{J}_{ij}\right)\mathbf{I} \\ \mathbf{J}_{ij}^{\mathrm{S}} = \frac{1}{2}\left(\mathbf{J}_{ij}+\mathbf{J}_{ij}^{T}\right)-\mathbf{J}_{ij}^{\mathrm{I}} \\ \mathbf{J}_{ij}^{\mathrm{A}} = \frac{1}{2}\left(\mathbf{J}_{ij}-\mathbf{J}_{ij}^{T}\right) \end{cases}$$

On-site anisotropy, *e.g.,* $K(\theta) = -K_2 \sin^2(\theta)$

Demonstrations of the relativistic effects:

- ***energy while rotating the whole configuration around the [100] axis.***
- ***expansion of the energy of the most symmetric atom in terms of the real sperical harmonics***

Global spin rotation around the [100] axis I.

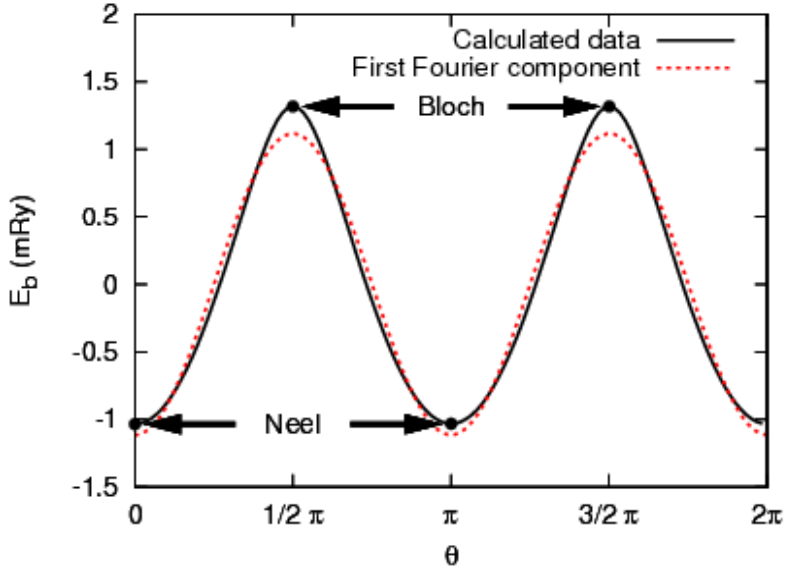

≈ uniaxial anisotropy

coordination number

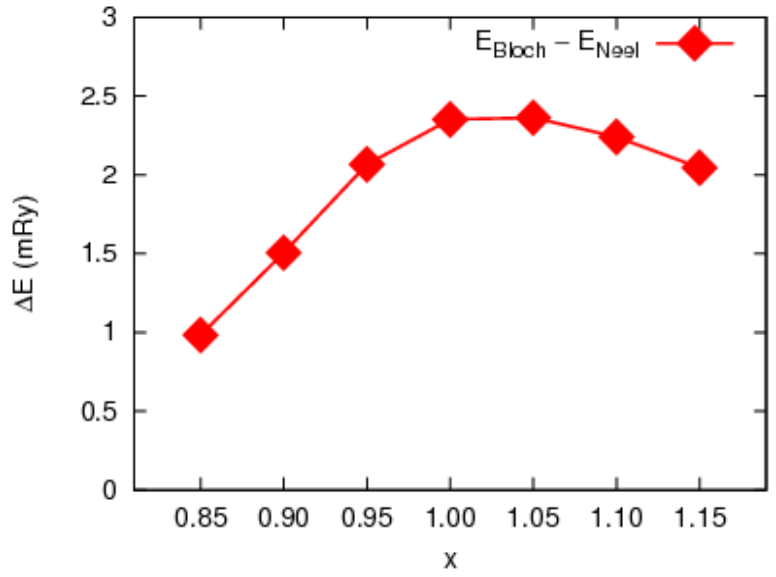

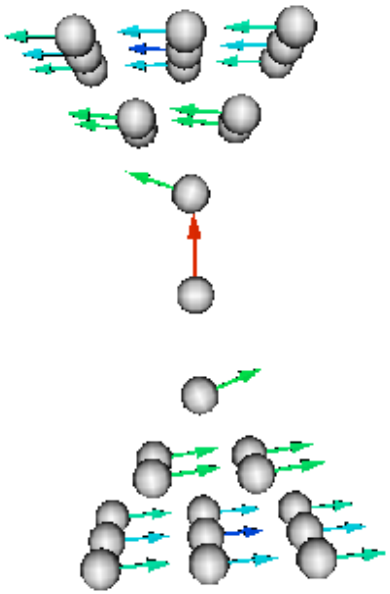

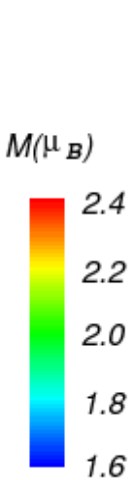

Bloch

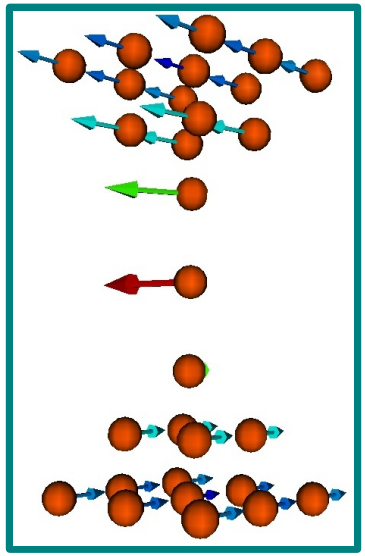

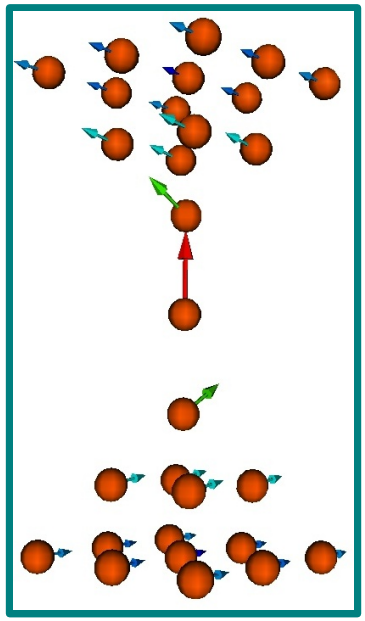

Néel

Global spin rotation around the [100] axis II.

TABLE I. Fourier components of the band energy while rotating all spins around the (100) direction as a function of the stretching paramerer, x. The displayed coefficients are the K_k coefficients in the expansion $E_\mathrm{b} = K_0 + \sum_{k=1}^{\infty} K_k \cos(k\theta)$. The other coefficients are practically zeros. The units are milli Rydberg.

x	$k=2$	$k=4$	$k=6$
0.85	−0.466	0.011	0.029
0.90	−0.735	0.026	0.037
0.95	−1.003	0.103	0.022
1.00	−1.116	0.159	−0.003
1.05	−1.112	0.173	−0.009
1.10	−1.055	0.164	−0.006
1.15	−0.967	0.141	0.002

Domain wall width

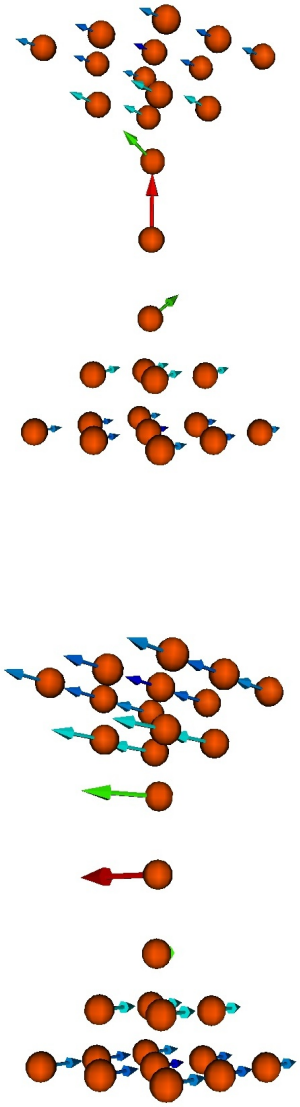

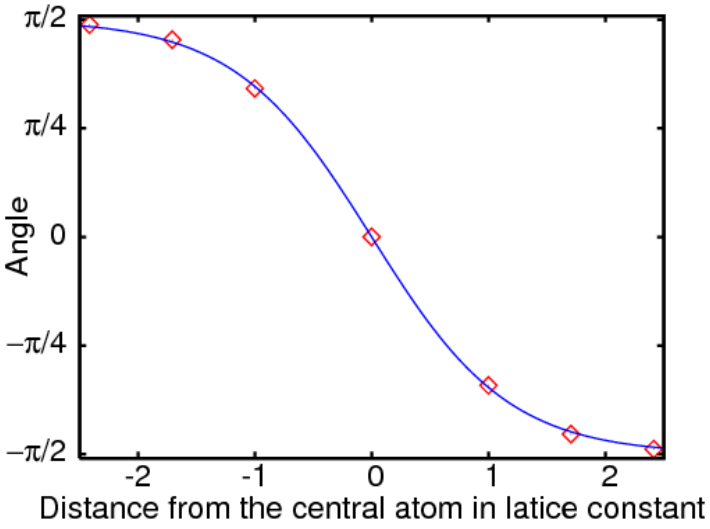

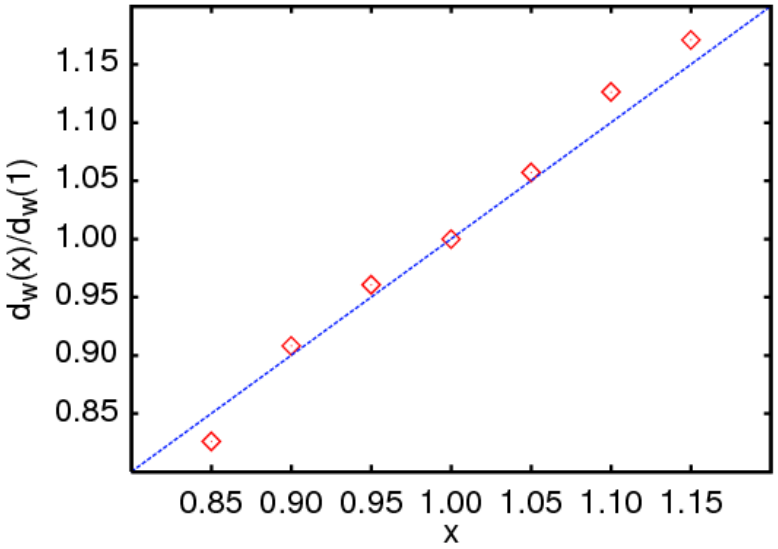

$$\varphi(z) = -\frac{\pi}{2}\mathrm{th}\left(\frac{z}{2d_{\mathrm{w}}}\right)$$

The geometry determines the domain wall width.

See: P. Bruno, PRL **83**, 2425 (1999).

Spin- and orbital moments

3. layer			2. layer		1. layer	central atom
1.85	1.78	1.85				
1.78	1.67	1.78	1.91	1.91	1.93	2.35
1.85	1.78	1.85	1.91	1.91		

3. layer			2. layer		1. layer	central atom
0.13	0.11	0.13				
0.10	0.07	0.10	0.13	0.13	0.16	1.71
0.13	0.11	0.13	0.13	0.13		

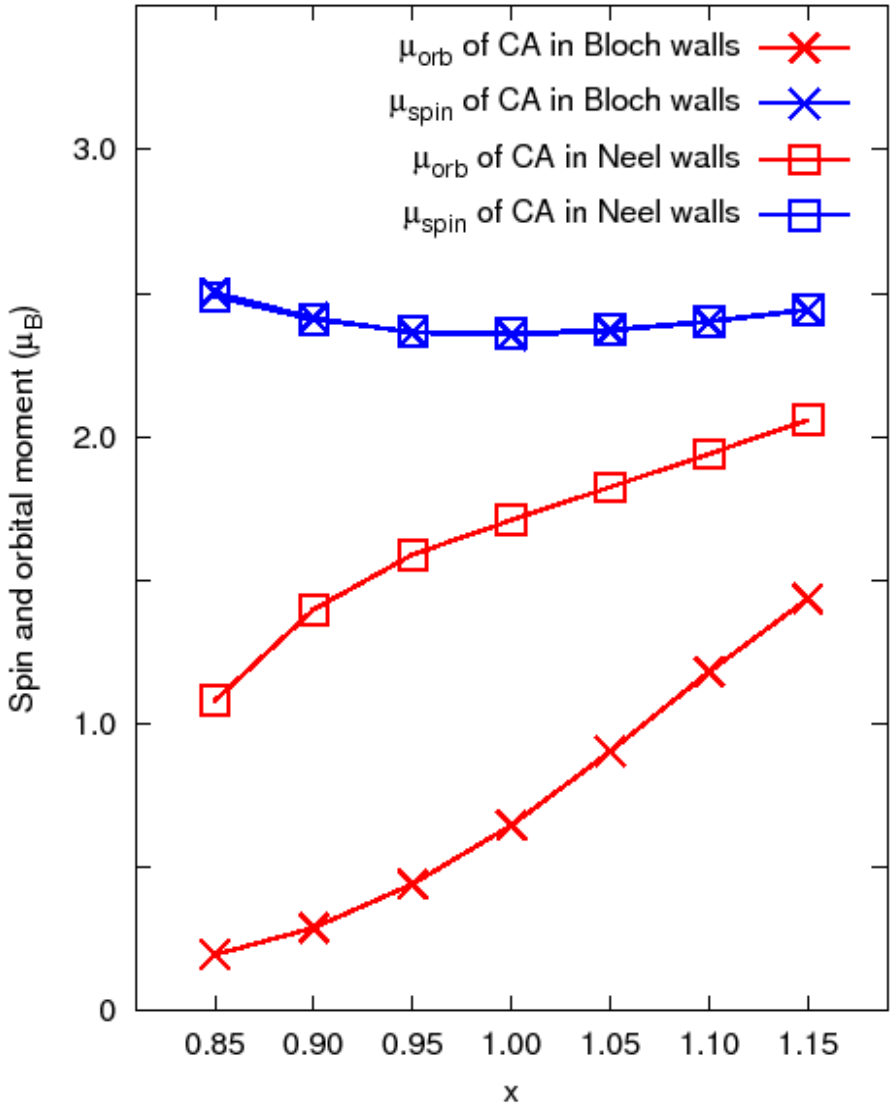

Modeling methods I.

Screened Korringa–Kohn–Rostoker / embedded cluster method [1]

Infinitesimal rotations method: [2]
► parameters of isotropic Heisenberg model

Monte Carlo: simulated annealing / Metropolis algorithm
► ≈ ground state

Minimization of the band energy by Newton−Raphson method
- frozen potential approximation

► ground state
► local quantities

Embedding + band energy calculation
- magnetic force theorem

► energy functions

[1] B. Lazarovits, *et. al.* PRB **65**, 104441 (2002)

[2] A.I. Liechtenstein *et al.* JMMM **67**, 65 (1987)
[2] L. Udvardi *et al.* PRB **68**, 104436 (2003)

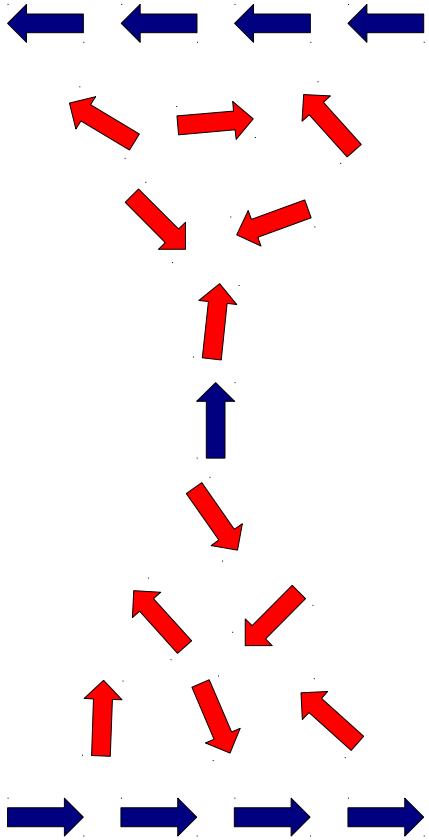

Embedding cluster method

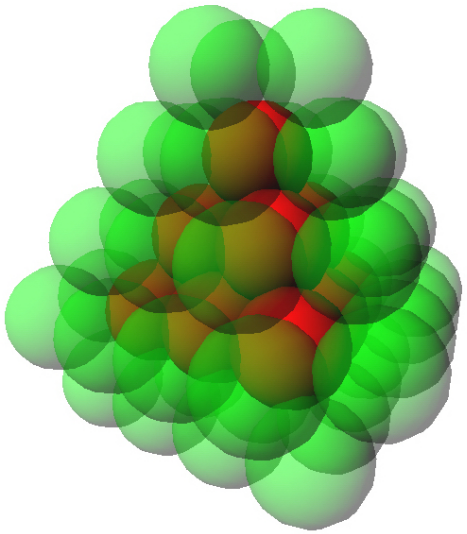

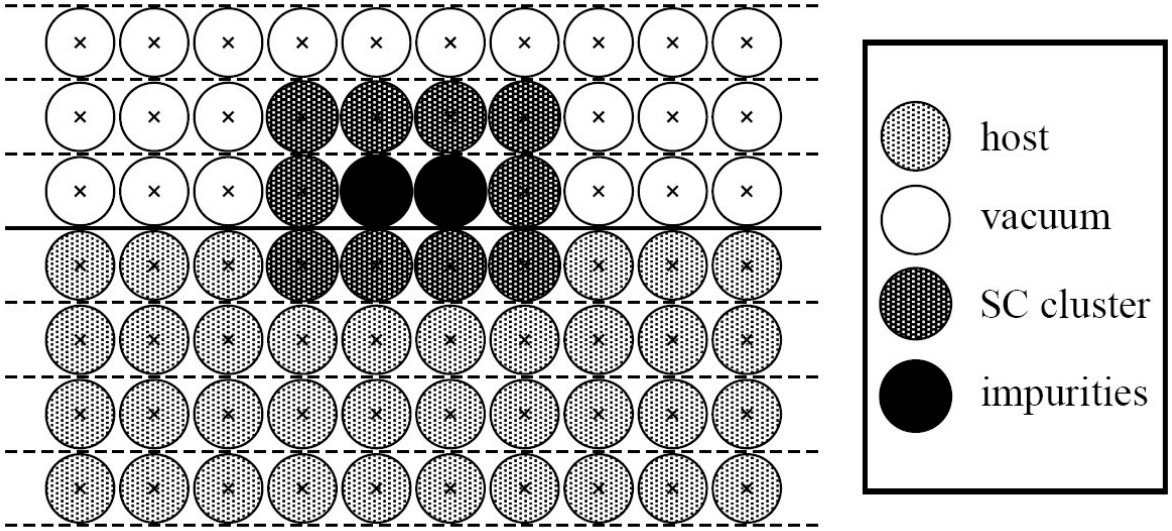

$$\boldsymbol{\tau}(\varepsilon) = \boldsymbol{\tau}_{\mathrm{host}}(\varepsilon)\left(\mathbf{I} - \Delta\mathbf{t}^{-1}(\varepsilon)\boldsymbol{\tau}_{\mathrm{host}}(\varepsilon)\right)^{-1}$$

Modeling methods II.

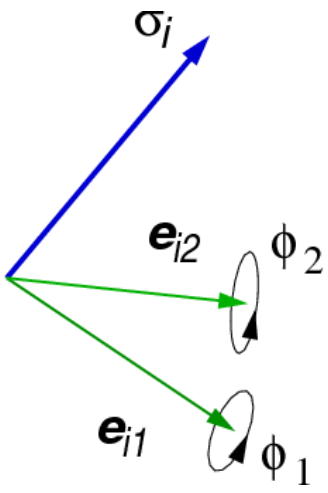

$$E_\mathrm{b} = \int_{-\infty}^{E_\mathrm{F}} (\varepsilon - E_\mathrm{F}) n(\varepsilon)\,\mathrm{d}\varepsilon = -\frac{1}{\pi}\mathrm{Im}\int_{-\infty}^{E_\mathrm{F}} \mathrm{Tr}\ln\tau(\varepsilon)\,\mathrm{d}\varepsilon$$

$$\frac{\partial E_\mathrm{b}}{\partial \phi_{i\alpha}} = \frac{1}{\pi}\mathrm{Im}\int_{-\infty}^{E_\mathrm{F}} i\,\mathrm{Tr}\left\{\tau_{ii}(\varepsilon)\left[\mathbf{e}_{i\alpha}\cdot\mathbf{J}, t_i^{-1}(\varepsilon)\right]\right\}\,\mathrm{d}\varepsilon$$

$$\frac{\partial^2 E_\mathrm{b}}{\partial\phi_{i\alpha}\,\partial\phi_{j\beta}} = \delta_{ij}\frac{1}{\pi}\mathrm{Im}\int_{-\infty}^{E_\mathrm{F}} \mathrm{Tr}\left\{\tau_{ii}(\varepsilon)\left[\mathbf{e}_{i\alpha}\mathbf{J}, \left[\mathbf{e}_{i\beta}\mathbf{J}, t_i^{-1}(\varepsilon)\right]\right]\right\}\,\mathrm{d}\varepsilon$$

$$-\frac{1}{\pi}\mathrm{Im}\int_{-\infty}^{E_\mathrm{F}} \mathrm{Tr}\left\{\tau_{ij}(\varepsilon)\left[\mathbf{e}_{j\beta}\mathbf{J}, t_j^{-1}(\varepsilon)\right]\tau_{ji}(\varepsilon)\left[\mathbf{e}_{i\alpha}\mathbf{J}, t_i^{-1}(\varepsilon)\right]\right\}\,\mathrm{d}\varepsilon$$

based on L. Udvardi *et al.* PRB **68**, 104436 (2003)

Self-consistent potential calculation

Newton−Raphson optimization of the directions

$$\mathbf{x}_{n+1} = \mathbf{x}_n - \frac{\mathrm{d}E_\mathrm{b}}{\mathrm{d}\mathbf{x}}\cdot\left(\frac{\mathrm{d}^2 E_\mathrm{b}}{\mathrm{d}\mathbf{x}^2}\right)^{-1}$$

Model of the energy function I.

$$E_{\text{band}}(\underbrace{\ldots}_{\text{fixed}}, \vartheta, \varphi, \underbrace{\ldots}_{\text{fixed}}) = \sum_{l=0}^{\infty} \sum_{m=-l}^{l} E_{lm} Y_{lm}(\vartheta, \varphi)$$

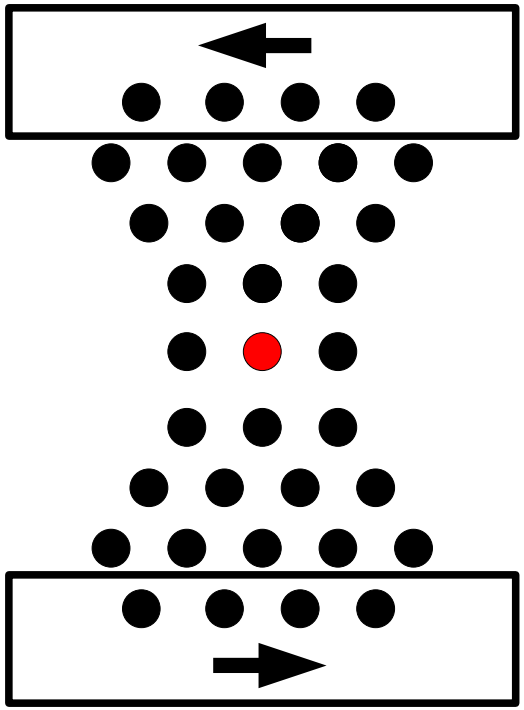

Model of the energy function II.

$$E_{\text{band}}(\underbrace{\ldots}_{\text{fixed}}, \vartheta, \varphi, \underbrace{\ldots}_{\text{fixed}}) = \sum_{l=0}^{\infty} \sum_{m=-l}^{l} E_{lm} Y_{lm}(\vartheta, \varphi)$$

l	m	R_l^m	Unit	$x = 1.00$
1	0	$\frac{1}{2}\sqrt{\frac{3}{\pi}}z$	mRyd	-15.61
2	0	$\frac{1}{4}\sqrt{\frac{5}{\pi}}\left(3z^2-1\right)$	mRyd	-2.38
2	2	$\frac{1}{4}\sqrt{\frac{15}{\pi}}\left(x^2-y^2\right)$	μRyd	38
3	0	$\frac{1}{4}\sqrt{\frac{7}{\pi}}\left(5z^3-3z\right)$	μRyd	52.1
3	2	$\frac{1}{4}\sqrt{\frac{105}{\pi}}\left(x^2-y^2\right)z$	μRyd	7.9
4	0	$\frac{3}{16}\sqrt{\frac{1}{\pi}}\left(35z^4-30z^2+3\right)$	μRyd	362
4	2	$\frac{3}{8}\sqrt{\frac{5}{\pi}}\left(x^2-y^2\right)\left(7z^2-1\right)$	μRyd	7.96
4	4	$\frac{3}{16}\sqrt{\frac{35}{\pi}}\left(x^4-6x^2y^2+y^4\right)$	μRyd	-3.0

Weiss field

crystal field → ionic anisotropy
(D_{4h} symmetry group)

other terms:
higher order spin—spin interaction

Similar uniaxial anisotropies can be found in:

Etz *et. al.,* PRB, **77,** 184425, (2008)
Bornemann *et. al.,* EuroPhys Journal D, **45,** 529, (2007)
Gambardella, *et. al.,* Science, **300,** 1130, (2003)

Model of the energy function III.

$$E_{\text{band}}(\underbrace{\ldots}_{\text{fixed}}, \vartheta, \varphi, \underbrace{\ldots}_{\text{fixed}}) = \sum_{l=0}^{\infty} \sum_{m=-l}^{l} E_{lm} Y_{lm}(\vartheta, \varphi)$$

TABLE II. Expansion coefficients of the band energy of the central atom according to real spherical harmonics. The units are indicated per row. (Note: all other coefficients not listed here are zeros.)

l	m	R_l^m	Unit	$x = 0.85$	$x = 0.90$	$x = 0.95$	$x = 1.00$	$x = 1.05$	$x = 1.10$	$x = 1.15$
1	0	$\frac{1}{2}\sqrt{\frac{3}{\pi}}z$	mRyd	−17.65	−18.12	−17.26	−15.61	−14.14	−12.94	−11.65
2	0	$\frac{1}{4}\sqrt{\frac{5}{\pi}}\left(3z^2-1\right)$	mRyd	−1.86	−2.20	−2.44	−2.38	−2.27	−2.09	−1.88
2	2	$\frac{1}{4}\sqrt{\frac{15}{\pi}}\left(x^2-y^2\right)$	μRyd	316	19	102	38	−21	−68	−100
3	0	$\frac{1}{4}\sqrt{\frac{7}{\pi}}\left(5z^3-3z\right)$	μRyd	302	225	119	52.1	−20.3	−105	−196
3	2	$\frac{1}{4}\sqrt{\frac{105}{\pi}}\left(x^2-y^2\right)z$	μRyd	−14.6	−6.8	0.3	7.9	14.4	19.6	21.5
4	0	$\frac{3}{16}\sqrt{\frac{1}{\pi}}\left(35z^4-30z^2+3\right)$	μRyd	−46	126	338	362	370	357	317
4	2	$\frac{3}{8}\sqrt{\frac{5}{\pi}}\left(x^2-y^2\right)\left(7z^2-1\right)$	μRyd	2.44	9.21	13.56	7.96	3.76	0.11	−3.82
4	4	$\frac{3}{16}\sqrt{\frac{35}{\pi}}\left(x^4-6x^2y^2+y^4\right)$	μRyd	−0.5	−0.4	−1.4	−3.0	−6.4	−13.7	−25.4

Mollweide-projection

How to plot an $E(\vartheta, \varphi)$ function?

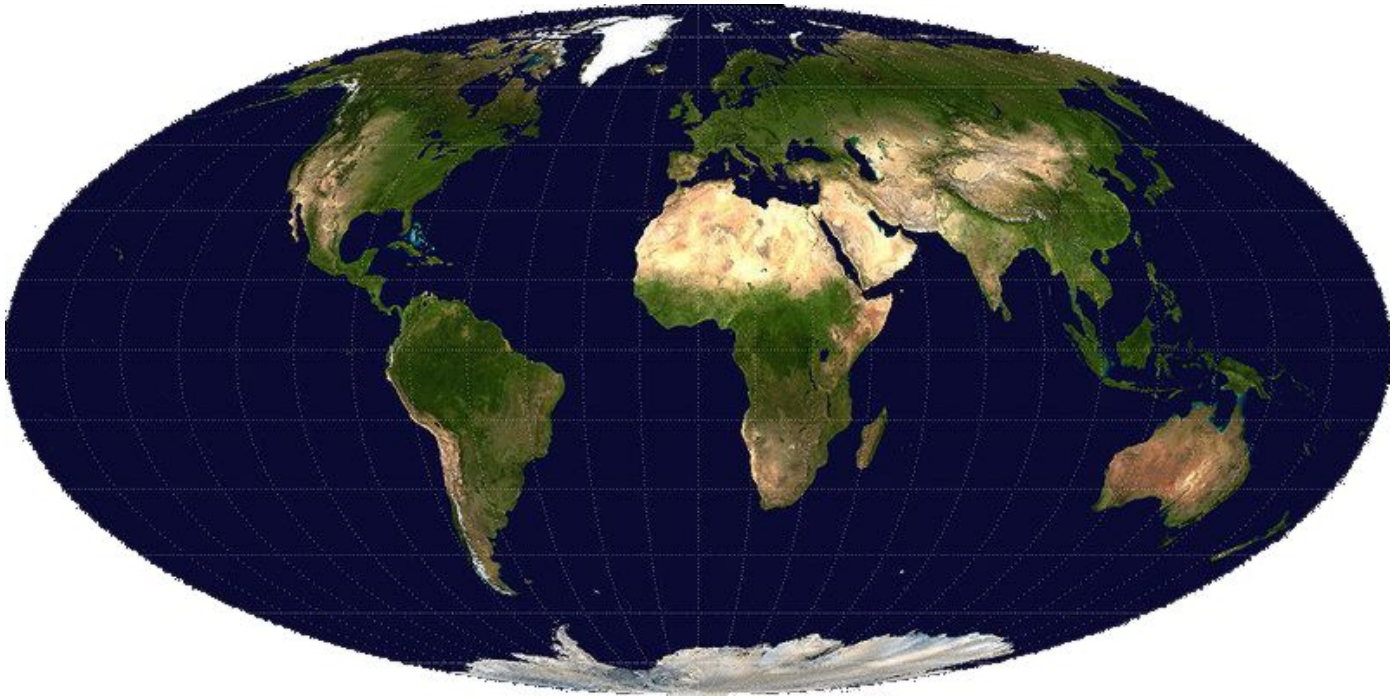

Mollweide-projection

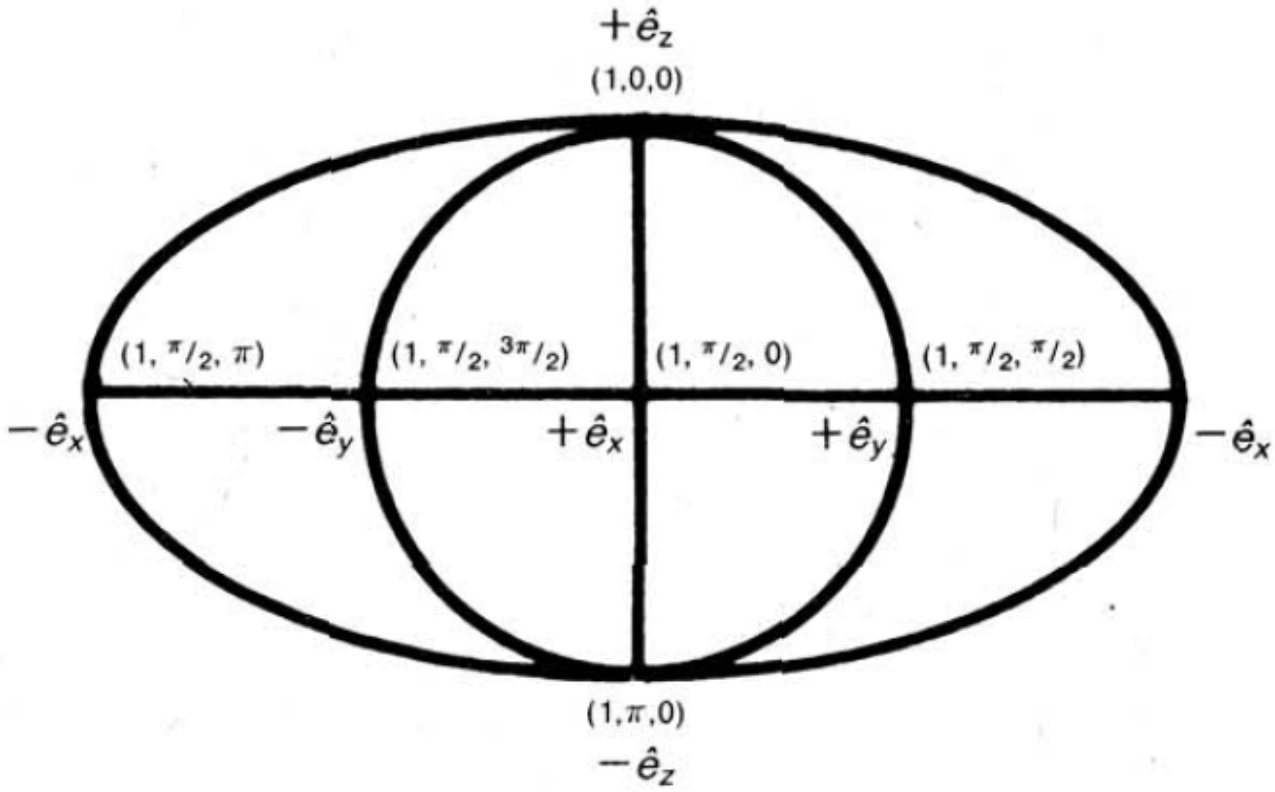

Figure 1. Mollweide's elliptical projection of the unit sphere based on the normal right-handed Cartesian coordinate system viewed towards the coordinate origin from along the $+x$ axis.

$$2\xi + \sin(2\xi) = \pi \cos(\vartheta)$$

$$x = 2\sqrt{2}\,\frac{\varphi}{\pi}\cos(\xi)$$

$$y = \sqrt{2}\sin(\xi)$$

C. M. Quinn *et al.*, J. Chem. Edu., **61,** 569, (1984)

http://en.wikipedia.org/wiki/Mollweide_projection

Decomposition of the energy function [Ryd]

$\ell = 1$

$-1.56 \cdot 10^{-2} \times$ 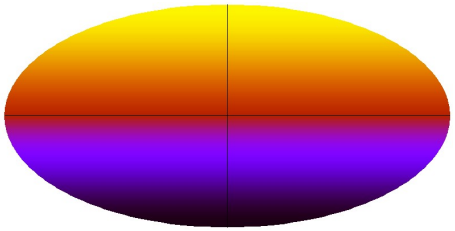

$\ell = 2$

$-2.38 \cdot 10^{-3} \times$ 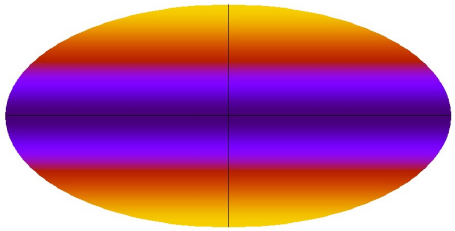

$3.75 \cdot 10^{-5} \times$ 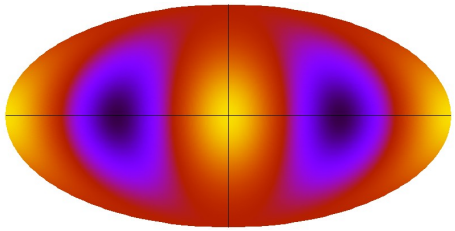

$\ell = 4$

$3.63 \cdot 10^{-4} \times$ 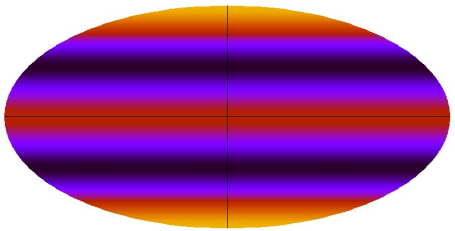

$7.96 \cdot 10^{-6} \times$ 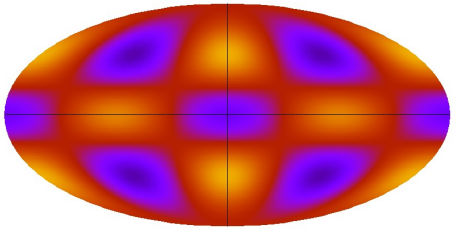

$-2.98 \cdot 10^{-6} \times$ 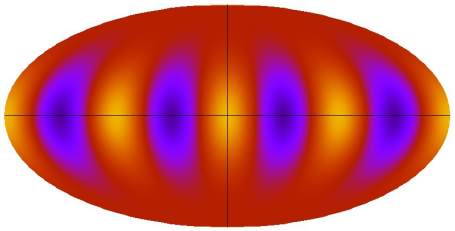

$\ell = 3$

$5.22 \cdot 10^{-5} \times$ 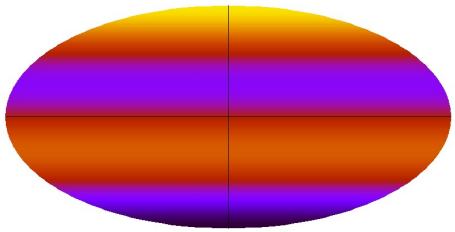

$7.91 \cdot 10^{-6} \times$ 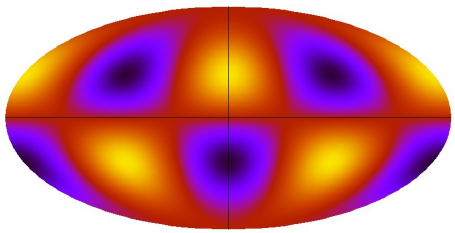

Decomposition of the energy function II.

$\ell = 1$

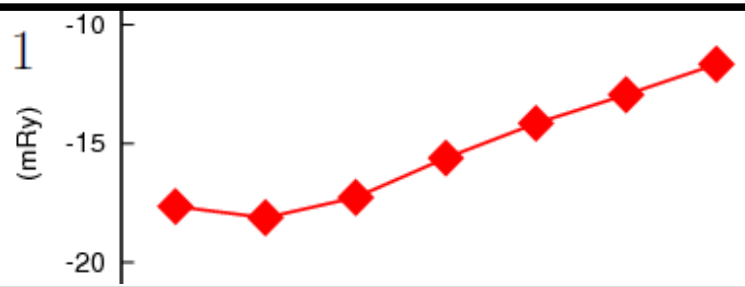

$\ell = 2$

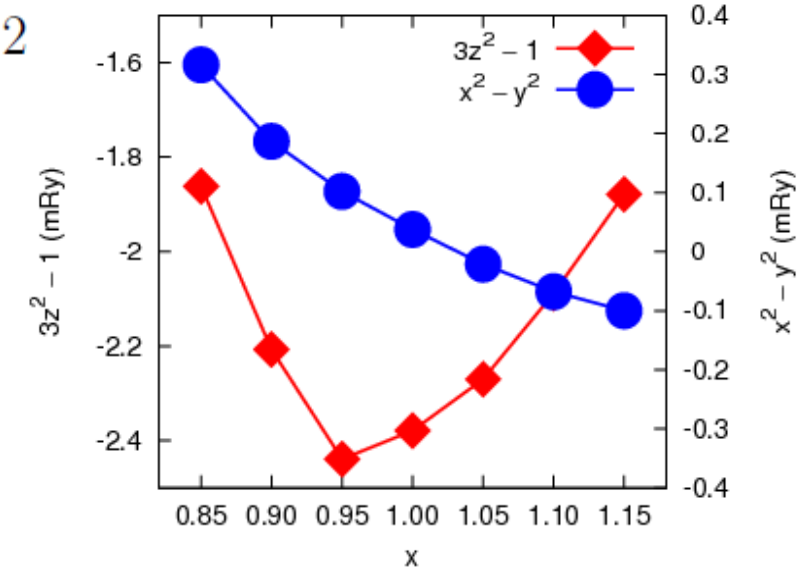

$\ell = 4$

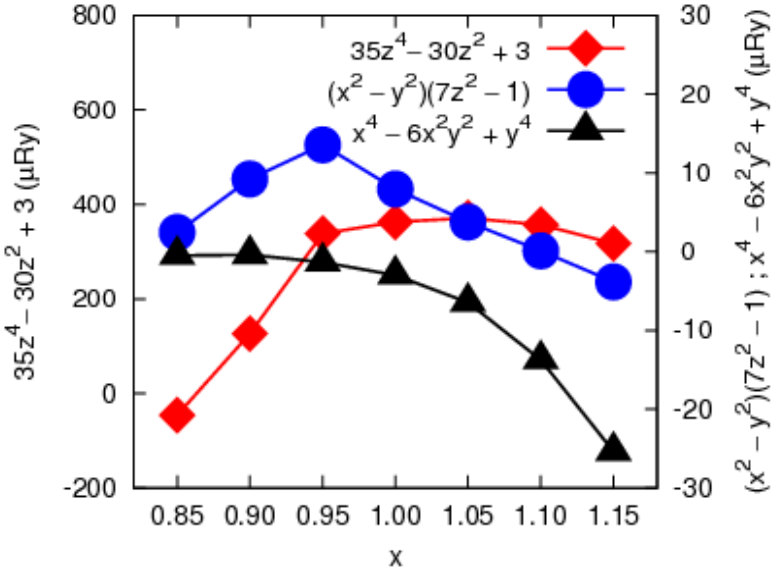

$\ell = 3$

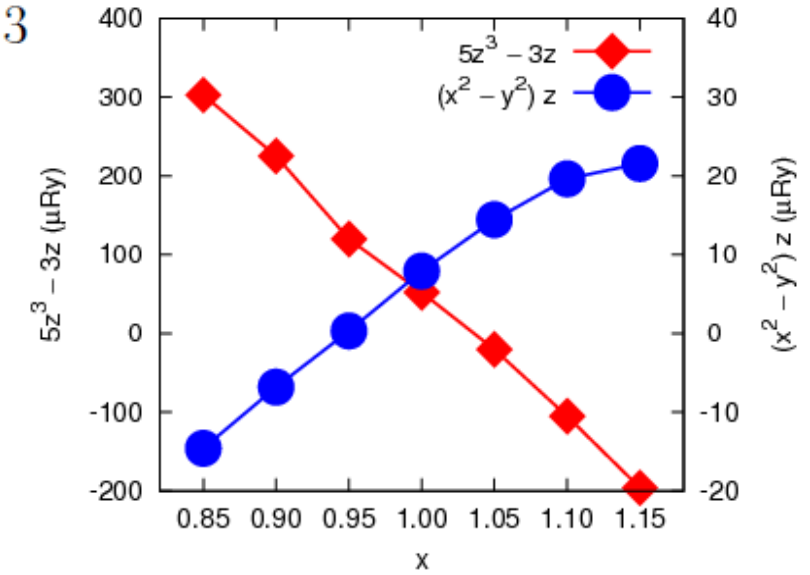

Where does the anisotropy come from?

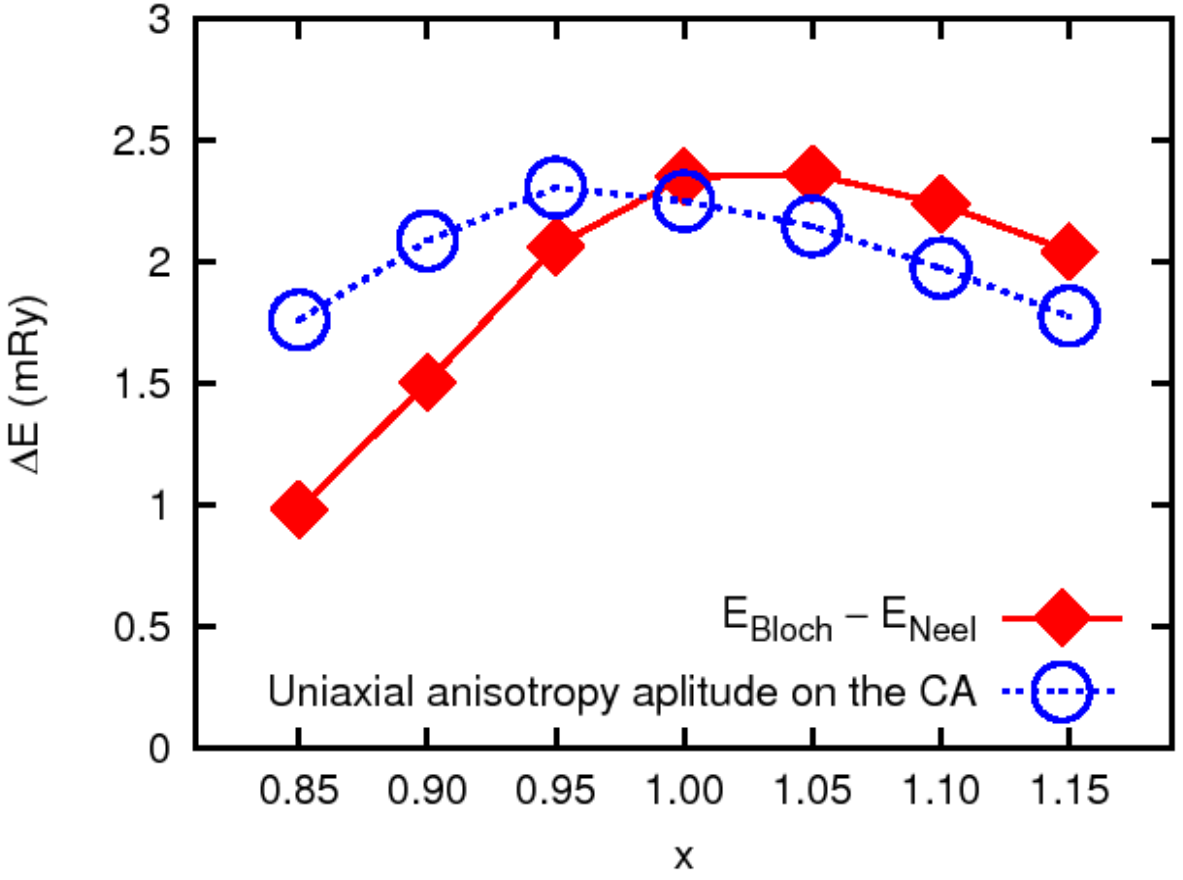

It is the on-site anisotropy which plays a stressed role in determining the ground state domain wall.

Summary

♣ A model of a cobalt nanocontact was constructed and investigated.

♣ The ground state was searched with multiscale approach: MC simulated annealing + NR optimization of the band energy.

♣ The Heisenberg model is not sufficient to map the magnetic energy landscape.

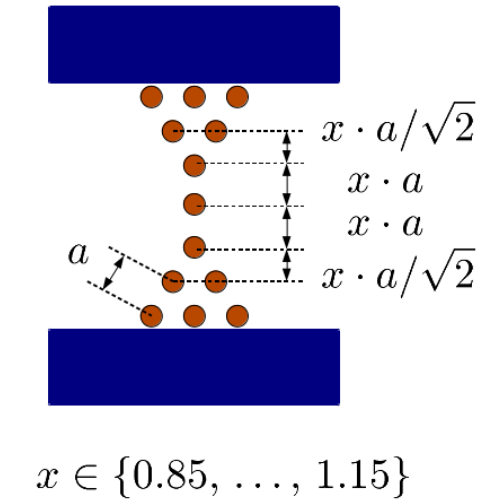

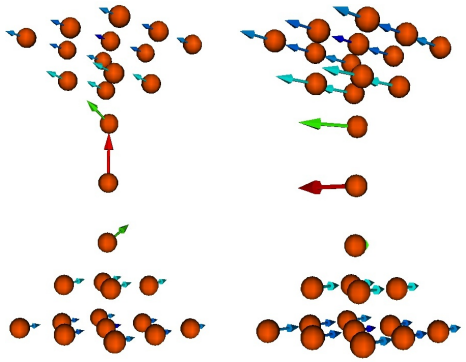

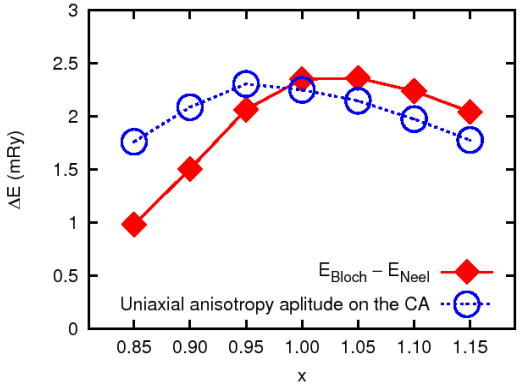

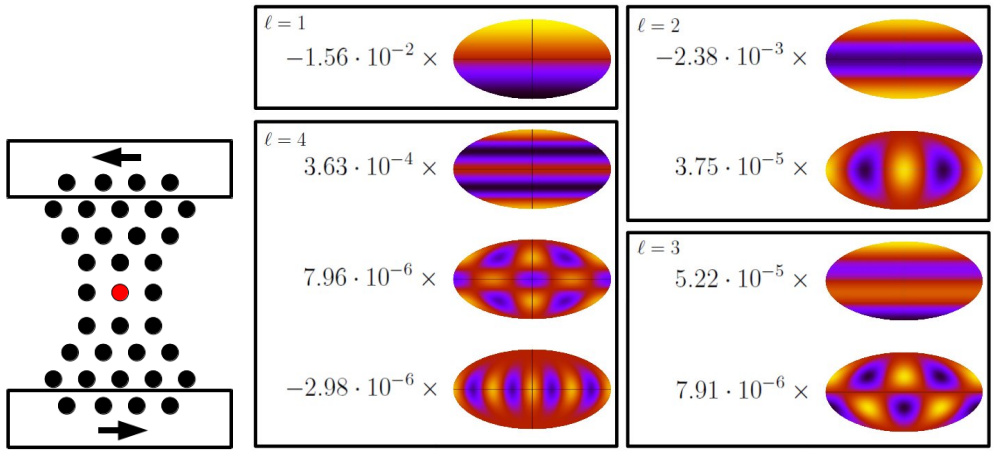

Future: Cr trimer on top of Au(111)

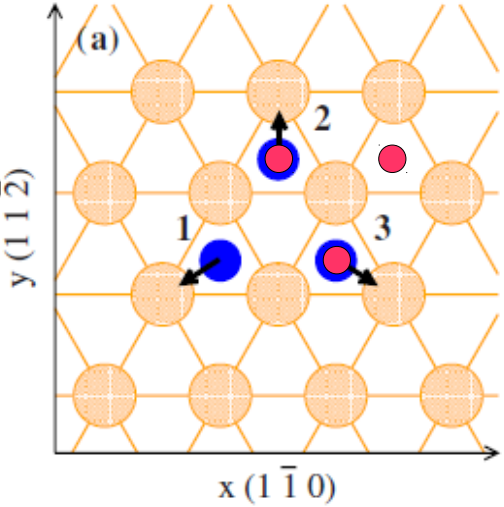

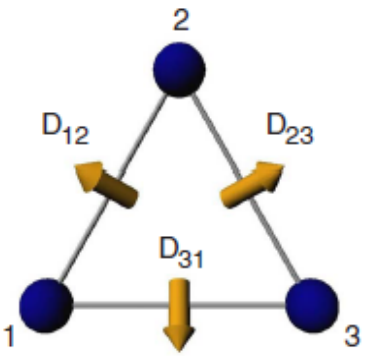

$$D_{12}=D_{13}=D_{23}=1.78 \text{ meV}$$

$$\vec{\kappa}=\frac{2}{3\sqrt{3}}\sum_{(ij)}(\vec{\sigma}_i\times\vec{\sigma}_j).$$

$$E_{\mathrm{DM}}=\frac{3\sqrt{3}}{2}D_z\kappa_z$$

$$\Delta E=5.04 \text{ meV}.$$

GROUND STATE

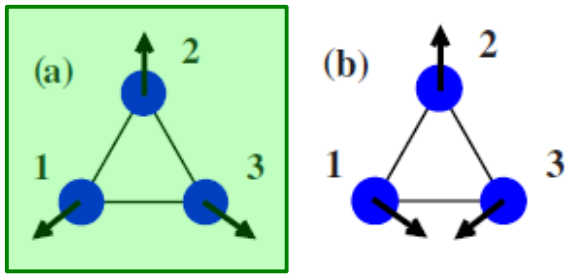

A. Antal, *et al.,* PRB, **77,** 174429, (2008)

From our global spin rotation idea, we also concluded that the ground state is the negative chirality state.

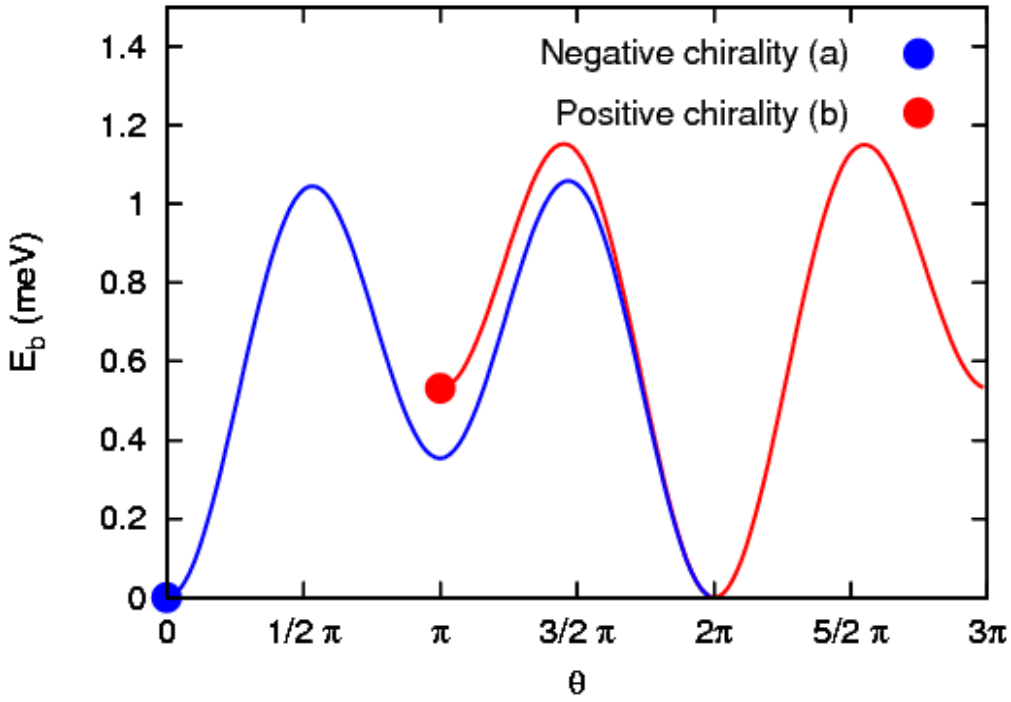

Next calculations:

– Cr trimer on different sites of the (111) surface

– search for the ground state using the self-consistent KKR + NR method

Thank you for your attention

László Balogh, Krisztián Palotás, Bence Lazarovits,
László Udvardi, László Szunyogh